Received: 15 June 2020 | Revised: 10 August 2020 | Accepted: 24 August 2020

DOI: 10.1096/fj.202001495R

RESEARCH ARTICLE

THE FASEB JOURNAL

Branched chain amino acids and carbohydrate restriction exacerbate ketogenesis and hepatic mitochondrial oxidative dysfunction during NAFLD

Muhammed S. Muyyarikkandy[1] | Marc McLeod[2] | Meghan Maguire[1] | Rohit Mahar[2] | Nathan Kattapuram[1] | Christine Zhang[1] | Chaitra Surugihalli[1] | Vaishna Muralidaran[1] | Kruthi Vavilikolanu[1] | Clayton E. Mathews[2] | Matthew E. Merritt[2] | Nishanth E. Sunny[1]

[1]Department of Animal and Avian Sciences, University of Maryland, College Park, MD, USA

[2]Department of Biochemistry and Molecular Biology, College of Medicine, University of Florida, Gainesville, FL, USA

Correspondence
Nishanth E. Sunny, Department of Animal and Avian Sciences, University of Maryland, College Park, MD 20742, USA.
Email: nsunny@umd.edu

Funding information
HHS | National Institutes of Health (NIH), Grant/Award Number: RO1-DK-112865, P41-122698, 5U2CDK119889 and R01-105346

Abstract

Mitochondrial adaptation during non-alcoholic fatty liver disease (NAFLD) include remodeling of ketogenic flux and sustained tricarboxylic acid (TCA) cycle activity, which are concurrent to onset of oxidative stress. Over 70% of obese humans have NAFLD and ketogenic diets are common weight loss strategies. However, the effectiveness of ketogenic diets toward alleviating NAFLD remains unclear. We hypothesized that chronic ketogenesis will worsen metabolic dysfunction and oxidative stress during NAFLD. Mice (C57BL/6) were kept (for 16-wks) on either a low-fat, high-fat, or high-fat diet supplemented with 1.5X branched chain amino acids (BCAAs) by replacing carbohydrate calories (ketogenic). The ketogenic diet induced hepatic lipid oxidation and ketogenesis, and produced multifaceted changes in flux through the individual steps of the TCA cycle. Higher rates of hepatic oxidative fluxes fueled by the ketogenic diet paralleled lower rates of de novo lipogenesis. Interestingly, this metabolic remodeling did not improve insulin resistance, but induced fibrogenic genes and inflammation in the liver. Under a chronic "ketogenic environment," the hepatocyte diverted more acetyl-CoA away from lipogenesis toward ketogenesis and TCA cycle, a milieu which can hasten oxidative stress and inflammation. In summary, chronic exposure to ketogenic environment during obesity and NAFLD has the potential to aggravate hepatic mitochondrial dysfunction.

KEYWORDS

fatty liver, hepatic insulin resistance, lipogenesis, liver mitochondria

Abbreviations: ALT, alanine aminotransferase; BCAAs, branched chain amino acids; BSA, bovine serum albumin; GC-MS, gas chromatography-mass spectrometry; HESI, Heated Electrospray Ionization; INCA, Isotopomer Network Compartmental Analysis; LC-MS/MS, liquid chromatography-mass spectrometry; NAFLD, non-alcoholic fatty liver disease; NASH, non-alcoholic steatohepatitis; NEFA, non-esterified fatty acids; OXPHOS, oxidative phosphorylation; PBS, phosphate-buffered saline; ROS, reactive oxygen species; SEM, standard error of means; SIM, single ion monitoring; SRM, selected reaction monitoring; TBDMS, tert-butyldimethylsilyl; TCA, tricarboxylic acid cycle; β-HB, β-hydroxybutyrate.

1 | INTRODUCTION

Alterations in mitochondrial oxidative metabolism are central features of hepatic insulin resistance contributing to the metabolic transition from simple steatosis to non-alcoholic steatohepatitis (NASH).[1-5] Normal hepatic mitochondrial function requires several metabolic networks including β-oxidation, ketogenesis, TCA cycle, oxidative phosphorylation (OXPHOS) and ATP synthesis to work in synergy in order to maintain cellular homeostasis. These oxidative networks adapt and remodel during the progressive severity of hepatic insulin resistance during NAFLD.[2,3,6] During early stages of NAFLD, there is an initial induction of components of the mitochondrial oxidative machinery (eg, ketogenesis, OXPHOS), which is followed by impairment of these networks during more severe stages of the disease. Such metabolic remodeling can occur simultaneously with the sustained induction of the hepatic TCA cycle.[1,7,8] More importantly, these disruptions in synergy between mitochondrial oxidative networks occur concurrent to lipid accumulation, higher rates of reactive oxygen species (ROS) generation and hepatocellular stress.[8,9] Under this scientific premise, a question which has remained unanswered is whether therapeutic, nutrient, or humoral induction of mitochondrial oxidative machinery during NAFLD is a beneficial strategy to alleviate metabolic dysfunction and lipid accumulation. Here, understanding the metabolic mechanisms which help to maintain the synergy between components of mitochondrial oxidative flux and hepatocellular stress is of great significance.

Ketogenic diets are popular means to enhance weight loss in humans.[10] While an array of dietary compositions can be ketogenic, most ketogenic diets employ a dietary macronutrient milieu containing high-fat (HF) calories together with low carbohydrate calories, and in many cases along with high dietary protein.[11,12] This macronutrient milieu has been demonstrated to induce high rates of lipid oxidation and in turn high rates of ketogenesis. Synthesis of ketones occur in the mitochondria when the acetyl-coA generated from β-oxidation of free fatty acids cannot be efficiently channeled through the TCA cycle for complete oxidation. Oxidation of BCAAs (leucine and isoleucine) and lysine can also contribute to ketogenesis. This is interesting in the context of the emerging roles of BCAAs in modulating lipid metabolism and the degree of insulin resistance.[13-16]

During the progression of NAFLD, sustained activity of mitochondrial oxidative metabolism (eg, TCA cycle) can contribute to chronic ROS generation and hepatocellular stress.[8,9] Moreover, the projected benefits of ketogenic diets are thought to be mediated by higher rates of lipid oxidation, in turn preventing lipid accumulation. This presents a conundrum on whether long-term exposure of the liver to a "ketogenic environment" will adversely impact mitochondrial oxidative function and insulin sensitivity during NAFLD.[17-22] This is a significant question to answer as prevalence of obesity is over 30% in the population and furthermore, over 70% of obese humans are susceptible to NAFLD.[23,24]

Toward our studies, we modified the rodent HF diet (60% fat calories; D12492, Research Diets) which is commonly used for the induction of NAFLD, by supplementing BCAAs (1.5X), specifically by replacing carbohydrate calories. Based on the above discussed scientific premises, we hypothesized that this custom diet will chronically induce ketogenesis in mice, and furthermore, worsen the severity of NAFLD. Long-term exposure of the mice to this modified diet resulted in a chronic ketogenic environment. Metabolic profiling demonstrated that chronic induction of hepatic mitochondrial oxidative networks (β-oxidation, ketogenesis, TCA cycle) occurred together with lower rates of lipogenesis in the liver of the ketogenic mice. This metabolic remodeling of the liver did not improve tissue specific insulin resistance, and furthermore, exacerbated the liver injury during NAFLD.

2 | MATERIALS AND METHODS

2.1 | Animals and diets

All the experiments were conducted in accordance with the Institutional Animal Care and Use Committee protocols approved at the University of Maryland, College Park. Male C57Bl/6NJ mice aged 6-8 weeks were purchased from Jackson Labs (Bar Harbor, ME) and were maintained (for 16-weeks) on a low-fat (LF) diet with 10% kcal from fat (D12450J, Research Diets, New Brunswick, NJ), a HF diet with 60% kcal from fat (D12492, Research Diets), or a HF diet with 150% BCAA supplementation by replacing carbohydrate calories (HF-Kt; D18060102, Research Diets). Detailed dietary composition can be found in Supporting Table S1. The HF-Kt diet was formulated with the specific intent of chronically inducing ketogenesis in the mice reared on this diet. Considering their ketogenic potential, and further their emerging relevance in the etiology of insulin resistance and dysfunctional lipid metabolism,[13-16] BCAA supplementation was selected as the replacement for carbohydrate calories toward formulating the HF-Kt diet. Mice were provided food and water ad libitum and maintained in a controlled 12-hour light/dark cycle. Metabolic studies were conducted as detailed below either under fed or after overnight food-restriction (15-18 h.).

2.2 | Stable isotope infusions for metabolite turnover

Following 16 weeks on custom diets, an indwelling jugular vein catheter was implanted and the mice were allowed to

recover for 4-5 days before stable isotope infusions. Stable isotope infusions were conducted under fed and food-restricted conditions. A subset of the food-restricted mice from all the three groups were also subjected to insulin stimulation (hyperinsulinemic euglycemic clamp). The mixture containing [$^{13}C_6$]glucose (24.4 μmoL/h), and [$^{13}C_4$]β-hydroxybutyrate (β-HB, 7.6 μmoL/h) (Cambridge Isotope Laboratories, Inc, Tewksbury, MA) was infused as a bolus for 10 minutes. This was followed by continuous infusion of these stable isotopes ([$^{13}C_6$]glucose: 9.8 μmoL/h, and [$^{13}C_4$]β-HB: 3.1 μmoL/h) for another 80 minutes to attain isotopic steady state. Toward the euglyceimic hyperinsulinemic clamp, insulin (2.5mU/kg/min) was infused at a constant rate along with β-HB: 3.0 μmoL/h). [$^{13}C_6$]glucose (9 mg/mL) was mixed with 30% dextrose solution and infused at variable rates to achieve euglycemia. Blood glucose levels were monitored from the tail vein snip every 10 minutes throughout the procedure. Following stable isotope infusions under fed, food-restricted and insulin stimulated conditions, blood was collected under isoflurane anesthesia, spun at 1500 g for 10 minutes to isolate serum which was frozen at −80ºC. Around 0.75-1.0 gram of the fresh liver was utilized immediately for isolated mitochondrial studies as detailed below and the remaining portion was flash frozen in liquid nitrogen and then at −80ºC for gene, protein and metabolite analysis.

2.3 | Isolated mitochondrial studies

Fresh liver from "Fed" and "Food-restricted" mice were washed with ice cold 1X phosphate-buffered saline (PBS) and then minced in 2-4 mL of MSHE buffer (70 mM sucrose, 210 mM mannitol, 5mM HEPES, 1 mM EGTA, and 0.5% bovine serum albumin (BSA); pH 7.2). The tissue was then homogenized in a Dounce homogenizer (3-5 strokes), transferred into a 15 mL falcon tube, diluted with 4mL of MSHE buffer and centrifuged at 800 *g* for 10 minutes at 4°C. The supernatant was then passed through a double-layered cheese cloth into a new 15 mL tube and centrifuged at 8000 *g* for 10 minutes at 4°C, to obtain the mitochondrial protein pellet. This pellet was then re-suspended in 3 mL of MSHE buffer and centrifuged again at 8000 *g* for 10 minutes at 4°C. This process was repeated to obtain the final mitochondrial pellet, which was then suspended in 100 μL of MSHE buffer without BSA. A 3-5 μL of aliquot of the mitochondrial pellet suspension was lysed in a lysis buffer to estimate mitochondrial protein content using Pierce protein assay kit (Thermo Fischer Scientific. Waltham, MA).

Isolated liver mitochondrial aliquots (500 μg) were incubated with 1mL of MAS-3 buffer (115 mM KCl, 10 mM KH2PO4, 2 mM MgCl2, 3 mM HEPES, 1 mM EGTA and 0.2% fat free BSA; pH 7.2) containing 2.5 mM malate and 20 μM palmitoyl carnitine, along with either 1mM [$^{13}C_3$] pyruvate or 1mM unlabeled pyruvate. Mitochondria were incubated for 0, 5 and 10 minutes at 37°C. Immediately following incubations, the mitochondria were pelleted by centrifugation at 8000 rpm for 5 minutes at 4°C. The mitochondrial pellet was then washed with 250 μL of cold 1X PBS, centrifuged at 8000 rpm for 2 minutes, and the supernatant was discarded before freezing the pellet at −80°C after the addition of 100 μL of cold methanol. The mitochondrial samples incubated with [$^{13}C_3$]pyruvate were analyzed to determine the incorporation of ^{13}C into the TCA cycle intermediates. Rates of biochemical reactions in the TCA cycle were determined from the mass isotopomer distribution arising from [$^{13}C_3$]pyruvate, using Isotopomer Network Compartmental Analysis (INCA) software as described below. The mitochondrial samples which were incubated with unlabeled pyruvate were utilized to determine the changes in pool sizes of the TCA cycle intermediates and amino acids. Metabolite pool sizes were normalized for the expression of COX IV protein per μg crude mitochondrial protein pellet.

2.4 | Analysis of organic acids and amino acids by gas chromatography-mass spectrometry (GC-MS)

For GC-MS analysis, the samples (mitochondria or liver tissue) were homogenized with 750 μL of chloroform: methanol (2:1) using bead mill for 30 sec and extracted with shaking for 1h. Aqueous metabolites were then extracted into 250 μL of water, transferred to a 1 mL of v-vial and dried under a stream of nitrogen. The samples were then converted to their oximes with 20 μL of 2% methoxamine hydrochloride in pyridine (W/V) and microwaving at 350 W for 90 sec. The samples were converted to their respective TBDMS (Tert-butyldimethylsilyl) derivatives at 90°C for 1 hour[25] The metabolites were separated on a HP-5MS UI column (30 m × 0.25 mm × 0.25 μm; Agilent, CA) and the ion fragments determined by single ion monitoring (SIM) under electron ionization mode using a GC-MS (5973N, Mass Selective Detector coupled to a 6890 Series GC System, Agilent, CA). Metabolite pool sizes were determined by comparing the area under the curve of the unlabeled ion fragment to their respective stable isotope-labeled internal standard, which was spiked into the sample at a known amount prior to sample processing. For determining the ^{13}C enrichment in organic acids and amino acids arising from [$^{13}C_3$]pyruvate, SIM was performed for each of the isotopomer fragments of interest.

2.5 | Modeling of flux through the hepatic TCA cycle

Fluxes through the hepatic TCA cycle were derived using INCA, a freely available simulation program written in

MatLab.[26] To simulate central metabolism in the mitochondria, a mathematical model that included TCA cycle metabolism, pyruvate and palmitoyl-carnitine import, β-oxidation, ketogenesis, and the components of the malate-aspartate shuttle and malate-citrate carrier, was implemented. The condensation of acetyl-CoA to generate ketones was also included in the model. Specific metabolic steps that produce NADH or $FADH_2$ were modeled, and subsequent stoichiometric consumption of O_2 by oxidative phosphorylation was assumed. Metabolic intermediates that were not detected by GC-MS analysis were not included in the model. For example, flux from citrate to α-ketoglutarate was modeled as a single step. Furthermore, the model could only incorporate ^{13}C label via metabolism of [$^{13}C_3$]pyruvate, either through pyruvate dehydrogenase or pyruvate carboxylase. Metabolite fractional enrichments were generated from inputting the specific metabolite mass isotopomer distribution from the mitochondrial incubations and the chemical formula of the known mass fragment into INCA's natural abundance correction function as previously described.[26,27] For deriving non-steady state estimates of metabolic flux, metabolite pool sizes were incorporated into the model. Inputs of pool sizes, fractional enrichment of the metabolic intermediates, and oxygen consumption at 0, 5, and 10 minutes were used for the INCA simulation.

2.6 | GC-MS analysis of ketones

Serum (25 μL) samples were deproteinized with cold acetonitrile and the supernatant was dried under nitrogen. β-hydroxybutyrate in the samples was then converted to the TBDMS derivatives at 90°C for 1 hour, separated on a HP-5MS UI column (30 m × 0.25 mm × 0.25 μm; Agilent, CA) and the ion fragments 275.1 through 279.1 monitored by SIM under electron ionization mode using a GC-MS (5973N, Mass Selective Detector coupled to a 6890 Series GC System, Agilent, CA). For experiments where [$^{13}C_4$]β-hydroxybutyrate was infused into the mice, this allowed us to determine the dilution of [$^{13}C_4$] β-hydroxybutyrate in the serum and in turn calculate the turnover rates of β-hydroxybutyrate. For the determination of β-hydroxybutyrate concentrations, serum (25 μL) was spiked with a known amount of [$^{13}C_4$]β-hydroxybutyrate. Concentrations of β-hydroxybutyrate in these samples were quantified by comparison to the [$^{13}C_4$]β-hydroxybutyrate internal standard.

2.7 | Hepatic mitochondrial respiration

Isolated hepatic mitochondria (250 μg) from food-restricted mice were allowed to respire in 1-ml of MAS-3 buffer containing 2.5 mM malate and 20 μM palmitoyl carnitine, using an oxygraph oxygen electrode system (Hansatech Instruments, Norfolk, England). Following measurement of the basal (state II) respiration, ADP stimulated (state III) respiration was measured after addition of 100 μM ADP. State IV respiration was measured after ADP depletion. Basal and ADP stimulated respiration rates were normalized for the expression of COX IV protein per μg crude mitochondrial protein pellet.

2.8 | Liquid chromatography-mass spectrometry (LC-MS/MS) analysis of liver acylcarnitines

Liver aliquots (~15-20 mg) from food-restricted mice were homogenized and deproteinized with cold acetonitrile containing a known amount of stable isotope-labeled acylcarnitine internal standard (Cambridge Isotopes, MA). The supernatant was dried and reconstituted in 90:10 of methanol-water for LC-MS/MS analysis. The data were collected using selected reaction monitoring (SRM) mode on a Thermo TSQ Quantum Access triple-quadrupole mass spectrometer with an Accela 1200 LC pump and Heated Electrospray Ionization (HESI) source (positive ionization). Reactions fragmenting to *m/z* 85.3 were monitored following a 5-μL injection on an ACE PFP-C18 column (100 × 2.1 mm, 2 μm particle size) at 40°C.[16]

2.9 | GC-MS analysis of serum glucose

Serum (25 μL) from food-restricted mice was spiked with [$^{13}C_6$] glucose (5.37 mM; Cambridge isotopes, MA), deproteinized with 500 μL of acetonitrile, and the supernatant dried under vacuum. The glucose was converted to its Di-O-isopropylidene derivative for GC-MS analysis using a HP-5MS UI column (30 m × 0.25 mm × 0.25 μm; Agilent, CA) under electron impact ionization (5973N, Mass Selective Detector coupled to a 6890 Series GC System, Agilent, CA).[25]

2.10 | De novo lipogenesis in the liver

Mice maintained on LF, HF, and HF-Kt diets were intraperitoneally injected with saline D_20 (27 μL/g body weight) and then maintained for 4 days on 4% D_20 in drinking water. "Fed" livers were collected and 1 g tissue was utilized to Folch extract the lipids with 20 ml of 2:1 chloroform: methanol. Liver lipids were dried and reconstituted in 180 μL of non-deuterated chloroform containing a pyrazine standard (4% pyrazine-d_4/96% pyrazine, 2 mg/mL), centrifuged and transferred into a 3 mm NMR tube. All ^1H and ^2H NMR spectra were recorded on a 14.1 T Bruker

Avance Neo system, equipped with 5 mm TXI CryoProbe. Proton and deuterium lock channel were used for acquiring the ^{1}H and ^{2}H NMR spectra, respectively. The standard proton pulse sequence was used to acquire ^{1}H NMR spectra of lipids at operating frequency of 600 MHz, consisting of 2 seconds relaxation delay (d1), 32 number of scans, 2 μs pulse width and 2 seconds acquisition time over a spectral width of 11 ppm. ^{2}H NMR spectra of lipid samples were acquired at operating frequency of 92.14 MHz with acquisition time of 2 seconds, relaxation delay of 2s, flip angle of 90°, 2048 number of scans, acquired size of 2173 data points with spectral width of 11 ppm. All NMR data were analyzed using the MestReNova v14.0.1-23284 (Mestrelab Research S. L.). The calculation of methyl ^{2}H-enrichment in lipids and de novo lipogenesis were done as previously described.[28,29]

2.11 | Liver histology

Livers (~150 mg) from food-restricted mice were fixed in 4% neutral buffered formalin for 18-24 hours, washed thrice and stored in 70% ethanol at 4°C. Masson's Trichrome staining of liver tissue (n = 3 per group) was performed by Histoserv, Inc, (Germantown, MD) to visualize lipid droplets and the fibrogenic foci.

2.12 | Gene expression analysis

Total RNA was extracted from frozen liver tissues (~15-20 mg) using 500 μL TRIZOL reagent (Invitrogen, Carlsbad, CA) and mRNA mini prep kit. The quality and concentration of mRNA was determined at OD 260/280 using Biotek take 3 plate reader. cDNA was prepared from1 μg mRNA using cDNA synthesis kit (Bio-Rad, Hercules, CA). Quantitative real-time PCR was performed on a Bio Rad CFX Real Time system (C1000 Touch Thermal Cycler) using 25 ng of cDNA, 150 nM of each primer, and 5 μL of SYBR green PCR master mix (Invitrogen, Carlsbad, CA) with cyclophilin (*Ppib*) as the housekeeping gene. For genes with low expression profiles (*IL6* and *TNFA*), gene specific Bio-Rad iselect cDNA synthesis kit (Bio-Rad Laboratories Inc, Hercules, CA) was used to amplify gene expression. The list of forward and reverse primers is provided in the Supporting Table S2.

2.13 | Protein estimation by western blot analysis

Frozen liver tissue (~20 mg) were lysed in a lysis buffer containing protease and phosphatase inhibitors and centrifuged at 15 000 rpm for 15 minutes. Total protein in the supernatant was measured using pierce BCA protein assay kit (Thermo Fischer Scientific. Waltham, MA). Proteins were separated using Bolt 8% Bis-tris Plus gels (Invitrogen, Carlsbad, CA) and was transferred to nitrocellulose membrane for incubation with primary antibodies for Akt, pAkt, COX IV and GAPDH (Cell signaling technology Inc, Danvers, MA).

2.14 | Biochemical assays

Plasma Non-esterified fatty acid (NEFA) concentrations were measured using HR Series NEFA-HR2 kit (WAKO diagnostics, CA). Plasma Insulin was measured by enzyme-linked immunoassay using (Crystal Chem USA, IL). Liver triglycerides concentrations were determined using an analytical kit (Serum triglyceride determination kit, Sigma-Aldrich, St. Louis, MO). Serum alanine aminotransferase (ALT) levels were determined using an analytical kit from Sigma-Aldrich, St. Louis, MO. All the procedures were done according to the manufacturer's protocol.

2.15 | Statistical analysis

All the data reported are presented as mean ± standard error of means (SEM), unless noted otherwise. Results were analyzed using one-way ANOVA, followed by a Tukey's multiple comparison test. Means were considered significantly different at $P \leq .05$, and trends were considered significant at $P \leq .1$. All statistical analysis were conducted and the graphs were plotted utilizing Prism 7 (GraphPad software Inc, San Diego, CA). For the TCA cycle flux analysis, the INCA software uses a Levenberg-Marquardt gradient descent algorithm to iteratively fit a least squares regression model as defined by the metabolic network to the inputs until a local minimum is achieved between experimental and simulated values.[26,30] This process was repeated 10 times before choosing the lowest energy option as previously described.[26,31] Subsequently, the proposed flux model is assessed for goodness of fit by a χ^2 test relative to the expected error. Upon generating a flux model that satisfies the χ^2 test, estimated flux 95% confidence intervals were calculated using the INCA parameter continuation function as earlier described.[26,31] Standard error was computed from the 95% confidence intervals by dividing the 95% confidence range by the two sided z-value, 3.92, as previously described.[30-32] The two sided z-value of 3.92 is achieved by multiplying the right sided tail z-value for the 95% confidence interval (1.96) two.[31,32] Estimated flux values and the computed standard error were plotted in Graphpad Prism 7.

3 | RESULTS

3.1 | Dietary supplementation of BCAAs by replacing carbohydrate calories resulted in a unique "Fed" vs "Food-restricted" metabolic phenotype

The metabolic characteristics of mice following 16-wks of LF, HF, and HF-Kt diets are detailed in Table 1. As expected, mice reared on HF diets had significantly higher body weights than their LF diet counterparts ($P \leq .05$). Interestingly, HF-Kt diet resulted in higher body weights (means ± SEM) compared to HF diets under both "Fed" (g; 40 ± 5 vs 46 ± 1; $P \leq .05$) and "Food-restricted" (g; 38 ± 1 vs 43 ± 1; $P \leq .05$) conditions. A comparison of the peri-gonadal adipose depots between HF and HF-Kt groups; "Fed" (g; 1.27 ± 0.10 vs 2.18 ± 0.12; $P \leq .05$) and "Food-restricted" (g; 1.25 ± 0.11 vs 1.43 ± 0.12; nonsignificant), suggest that the higher body weights in the HF-Kt group could be due to increased adiposity in these mice. The liver weights, serum insulin, and liver triglycerides revealed a distinctive metabolic phenotype following 16-wks of HF-Kt diet. As expected, all these measures were significantly higher in the "Fed" mice reared on HF diet compared to their LF counterparts (Table 1). However, HF-Kt diet reduced the liver weight (g; 2.6 ± 0.1 vs 1.8 ± 0.1; $P \leq .05$), lowered plasma insulin levels (ng/mL; 6.0 ± 0.8 vs 2.3 ± 0.3; $P \leq .05$) and resulted in lower liver triglyceride content (mg/ g liver; 147 ± 10 vs 66 ± 14; $P \leq .05$) under "Fed" conditions, relative to HF diet feeding. Surprisingly, under "Food-restricted" conditions, these seemingly beneficial trends from "Fed" state reversed, with the HF-Kt mice have higher liver weights (g; 1.3 ± 0.1 vs 1.5 ± 0.1; $P \leq .05$), similar fasting insulin levels (ng/mL; 0.7 ± 0.3 vs 0.6 ± 0.2) and higher liver triglycerides (mg/ g liver; 53 ± 12 vs 79 ± 5; $P \leq .05$) than their HF diet counterparts. Fasting serum glucose levels were lower in the HF-Kt mice than their HF counterparts (mg/dL; 126 ± 5 vs 109 ± 4; $P \leq .05$).

3.2 | Sixteen weeks on the HF-Kt diet resulted in chronic induction of ketogenesis

Rates of whole body ketone turnover were determined from the dilution of [$^{13}C_4$]β-hydroxybutyrate tracer in serum.

TABLE 1 Metabolic characteristics of mice reared on LF, HF, and HF-Kt diets for 16 weeks

	Feeding status	LF	HF	HF-Kt
Body weight (g)	Fed (n = 13-15)	29.2 ± 0.5	40.3 ± 4.6^{a}	46.1 ± 0.7^{bc}
	Food-restricted (n = 13-15)	26.1 ± 0.5	38.1 ± 1.2^{a}	43.2 ± 0.7^{bc}
Liver weight (g)	Fed (n = 9)	1.50 ± 0.06	2.59 ± 0.12^{a}	1.82 ± 0.09^{ce}
	Food-restricted (n = 13-15)	1.06 ± 0.04	1.26 ± 0.09^{d}	1.52 ± 0.06^{bc}
Peri-gonadal adipose tissue (g)	Fed (n = 9)	0.93 ± 0.13	1.27 ± 0.10^{a}	2.18 ± 0.12^{bc}
	Food-restricted (n = 13-15)	0.44 ± 0.05	1.25 ± 0.11^{a}	1.43 ± 0.12^{b}
Serum glucose (mg/dL)	Food-restricted (n = 13-15)	113.1 ± 2.9	126.4 ± 5.4^{d}	109.1 ± 4.2^{c}
Serum insulin (ng/mL)	Fed (n = 6-7)	0.46 ± 0.06	5.96 ± 0.81^{a}	2.28 ± 0.27^{bc}
	Food-restricted (n = 6-7)	0.22 ± 0.05	0.68 ± 0.31	0.58 ± 0.15
Serum NEFA (mM)	Fed (n = 6-7)	0.49 ± 0.04	0.48 ± 0.03	0.46 ± 0.03
	Food-restricted (n = 6-7)	0.84 ± 0.07	0.65 ± 0.09^{d}	0.80 ± 0.05
Liver TGs (mg/g liver)	Fed (n = 8-9)	38.3 ± 10.1	147.1 ± 9.5^{a}	66.3 ± 14.4^{c}
	Food-restricted (n = 6-7)	47.7 ± 8.6	53.1 ± 12.4	78.5 ± 5.0^{ef}
Liver protein (mg/g liver)	Fed (n = 9)	185.1 ± 7.7	166.4 ± 8.4	192.4 ± 8.7^{f}
	Food-restricted (n = 13-15)	153.3 ± 11.5	145.8 ± 14.5	160.2 ± 9.6

All the values are expressed as means ± SEM. Significance at $P \leq .05$ following pairwise mean comparisons are represented by the alphabets. "a"—LF vs HF; "b"—LF vs HF-Kt; "c"—HF vs HF-Kt. Significance at $P \leq .1$ following pairwise mean comparisons are represented by the alphabets "d"—LF vs HF; "e"—LF vs HF-Kt; "f"—HF vs HF-Kt. TG, triglycerides; NEFA, non-esterified fatty acids.

Whole body turnover rates of β-hydroxybutyrate were significantly higher in mice reared on the HF-kt diet compared to their LF and HF counterparts during fed, food-restricted and insulin stimulated conditions (Figure 1A.). Turnover rates of β-hydroxybutyrate remained similar between mice reared on LF and HF diet (Figure 1A.). Fed to food-restricted

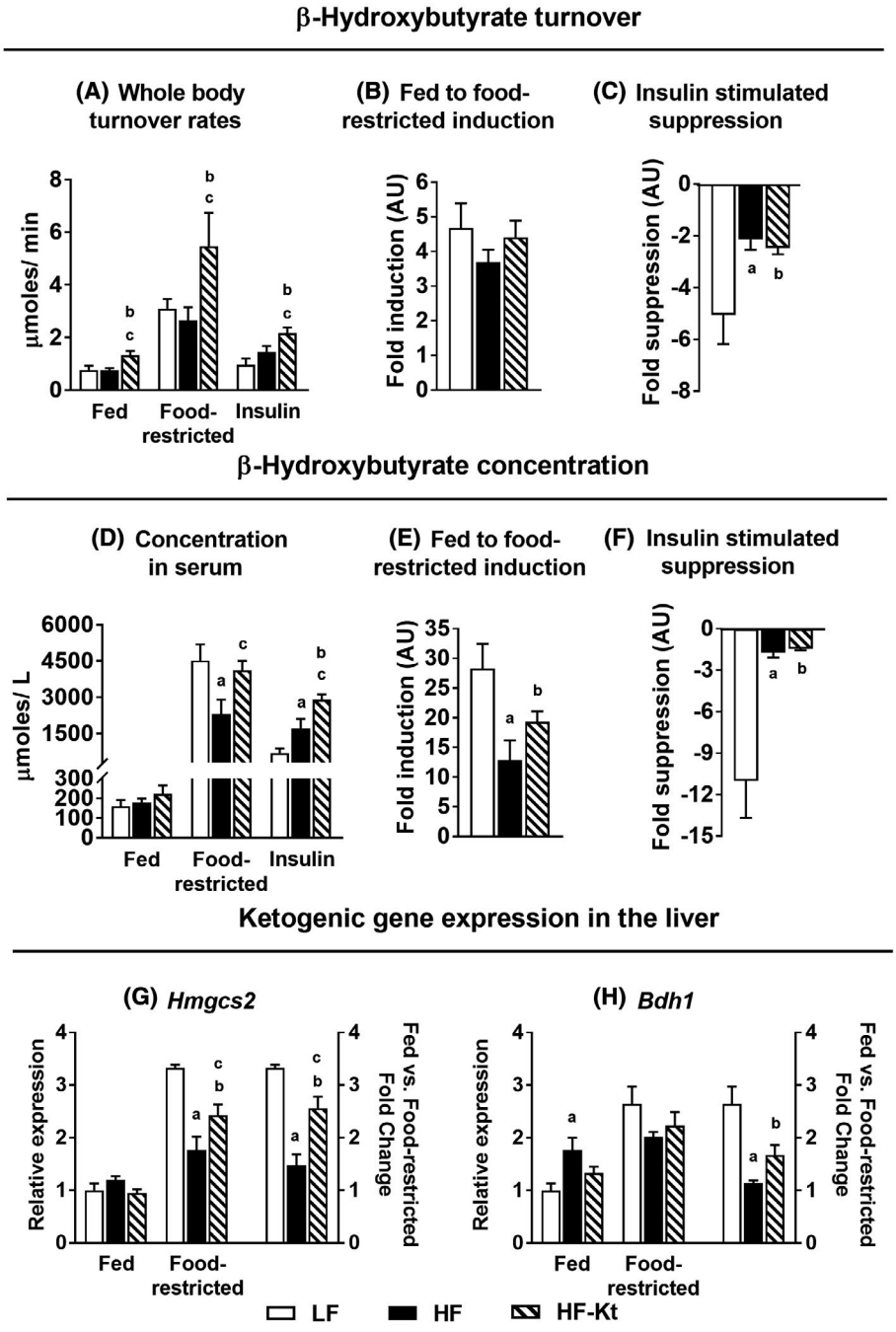

FIGURE 1 Chronic induction of ketogenesis following carbohydrate restriction and BCAA supplementation. A, Whole body β-hydroxybutyrate turnover rates during fed, food-restricted and insulin stimulated states. B, Fed to food-restricted induction of β-hydroxybutyrate turnover. C, Insulin stimulated suppression of β-hydroxybutyrate turnover. D, Serum β-hydroxybutyrate concentration during fed, food-restricted and insulin stimulated states. E, Fed to food-restricted induction of serum β-hydroxybutyrate concentrations. F, Insulin stimulated suppression of serum β-hydroxybutyrate concentrations. G, Gene expression profile of *Hmgcs2,* 3-hydroxy-3-methylglutaryl-Coenzyme A synthase 2 and (H) Gene expression profile of *Bdh1,* 3-hydroxybutyrate dehydrogenase, type 1. Gene expression profiles are relative to the LF fed group. Results (n = 6-9/group) were considered significant at $P \leq .05$ following pairwise mean comparisons which are represented by the following alphabets. "a"—LF vs HF; "b"—LF vs HF-Kt; "c"—HF vs HF-Kt

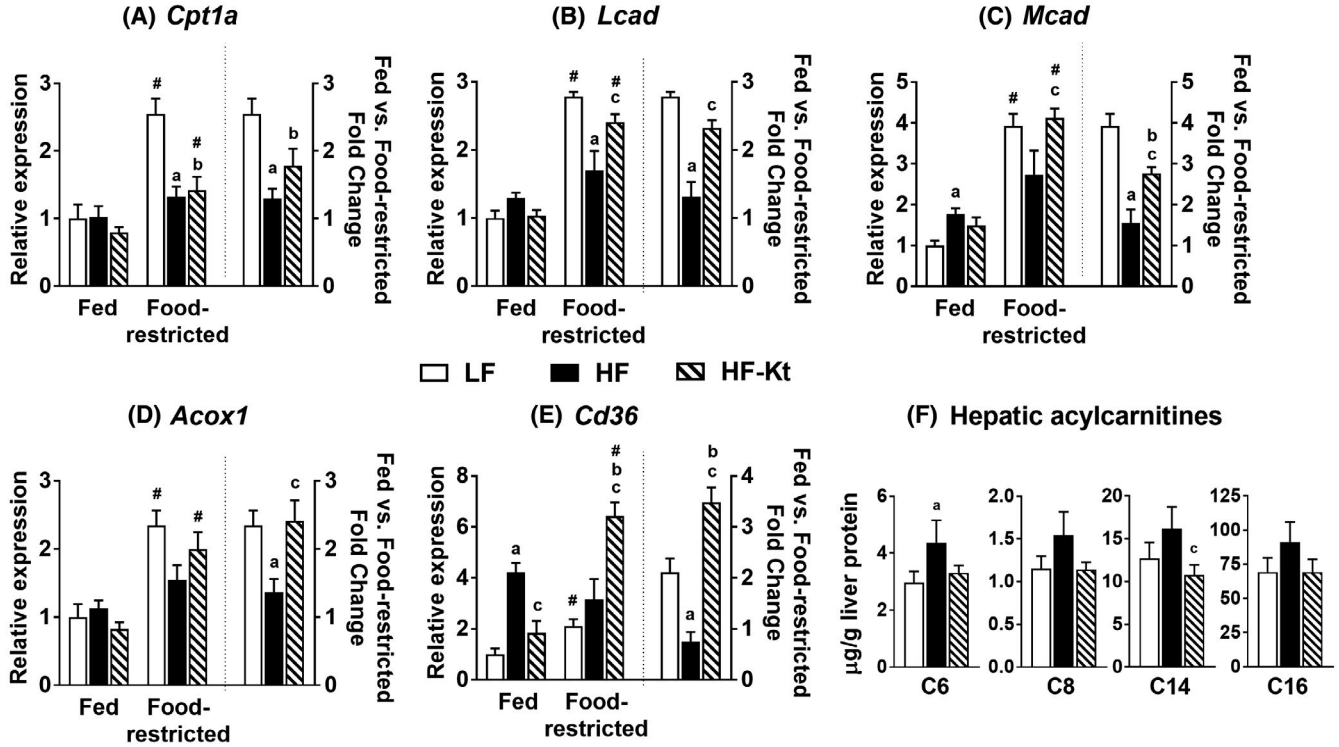

FIGURE 2 The ketogenic dietary environment results from the induction of hepatic β-oxidation. RT-qPCR assay profiles of genes involved in hepatic β-oxidation under fed and food-restricted conditions are represented on the left y-axis and the fold change in expression profiles from feeding to food-restriction are represented on the right y-axis. Gene expression profiles are relative to the LF "Fed" group. A, *Cpt1a,* carnitine palmitoyltransferase 1a (B) *Lcad,* Long-chain acyl-CoA dehydrogenase (C) *Mcad,* Medium-chain acyl-CoA dehydrogenase (D) *Acox1,* acyl-Coenzyme A oxidase 1 and (E) *Cd36,* CD36 molecule. F, Hepatic acyl-carnitine levels in food-restricted livers; C6, C8, C14, and C16 are hexanoyl- octanoyl-, myristoyl,- and palmitoyl-carnitines, respectively. Results (n = 6-9/group) were considered significant at $P \leq .05$ following pairwise mean comparisons which are represented by the following alphabets. "a"—LF vs HF; "b"—LF vs HF-Kt; "c"—HF vs HF-Kt. "#"—indicates statistical significance at $P \leq .05$ using a Student's t test between the means of the "Fed" and "Food-restricted" groups

induction of β-hydroxybutyrate turnover remained similar between all the three groups (Figure 1B.). Insulin infusion significantly suppressed β-hydroxybutyrate turnover in LF mice by five-fold. Insulin mediated suppression of β-hydroxybutyrate turnover was significantly blunted in both HF and HF-kt mice (Figure 1C only ~2-fold suppression). Postprandial β-hydroxybutyrate concentrations were not significantly different between treatments (Figure 1D). However, food-restriction resulted in ~27-fold, 14-fold and 18-fold increase in serum β-hydroxybutyrate levels in LF, HF, and HF-kt groups, respectively (Figure 1E). By pairwise mean comparison, both food-restricted and insulin stimulated serum β-hydroxybutyrate concentrations were significantly higher in the HF-kt mice compared to their HF counterparts (Figure 1D). As expected, insulin stimulation significantly suppressed serum β-hydroxybutyrate levels in LF mice (by 11-fold). However, this suppression was significantly blunted in both HF and HF-kt mice (only two-fold suppression; Figure 1F). Hepatic expression of key ketogenic genes *Hmgcs2* and *Bdh1* were significantly induced by food-restriction, especially in the LF livers (3 to 3.5-fold). This response was blunted in HF (1.5-fold) and HF-Kt (2 to 2.5-fold) mouse livers (Figure 1G,H). More importantly, the feeding to food-restriction fold induction of *Hmgcs2* was significantly higher in the HF-Kt liver compared to their HF counterparts (Figure 1G.). A similar trend was evident with *Bdh1* gene expression, although not statistically significant (Figure 1H.). Taken together, the above results illustrate that BCAA supplementation together with carbohydrate restriction (HF-Kt diet) made the diet more ketogenic, resulting in chronic upregulation of ketogenesis.

3.3 | The ketogenic dietary environment induced fatty acid oxidation in the liver during "Fed" to "Food-restricted" transition

To determine whether the chronic induction in ketone turnover in the HF-Kt liver is fueled by higher rates of fatty acid oxidation, expression profiles of major genes involved in this process were determined during fed and food-restricted conditions. All the gene expression profiles were normalized relative to that of the LF-"fed" mice livers. On a LF diet, the expression of all the genes were significantly induced

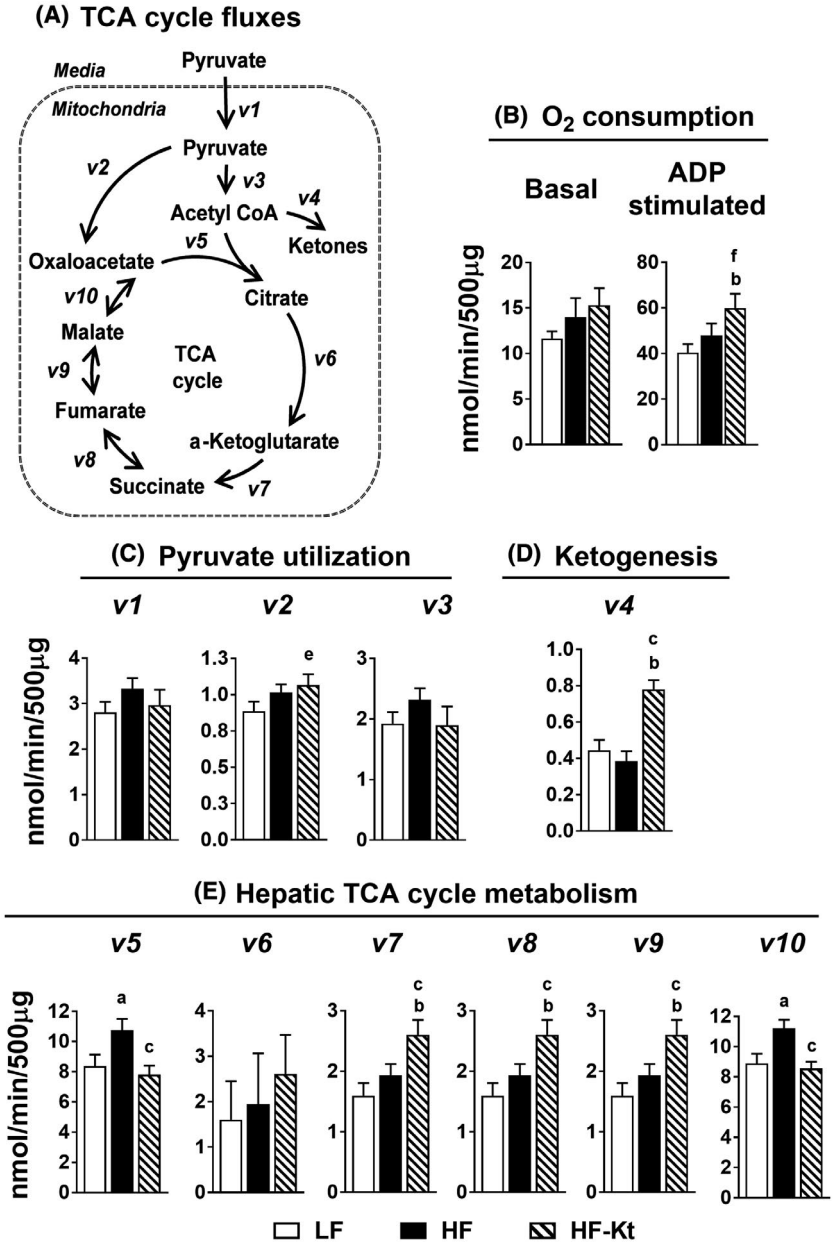

FIGURE 3 Impact of the ketogenic diet on the hepatic TCA cycle in mice with NAFLD. A, Mathematical modeling of the biochemical reactions in the TCA cycle. B, Basal and ADP stimulated O_2 consumption rates by the isolated mitochondria. C, Rates of pyruvate utilization by the isolated mitochondria; *v1* = rate of pyruvate entry into the mitochondrial matrix from the respiration buffer, *v2* = pyruvate carboxylation to form oxaloacetate, *v3* = formation of acetyl-CoA from pyruvate. D, Condensation of two acetyl-CoA molecules to form a β-hydroxybutyrate (Ketogenesis; *v4*). E, Rates of biochemical reactions in the hepatic TCA cycle; *v5* = condensation of acetyl-CoA and oxaloacetate to form citrate; citrate synthase flux, *v6* = formation of α-ketoglutarate from citrate, *v7* = formation of succinate from α-ketoglutarate, *v8* = reversible conversion of succinate to fumarate, *v9* = reversible conversion of fumarate to malate, *v10* = formation of oxaloacetate from malate. Calculated rates (n = 6-7/group) which are significant at $P \leq .05$ following pairwise mean comparisons are represented by the following alphabets. "a"—LF vs HF; "b"—LF vs HF-Kt; "c"—HF vs HF-Kt. Calculated rates (n = 6-7/group) which are significant at $P \leq .1$ following pairwise mean comparisons are represented by the following alphabets. "d"—LF vs HF; "e"—LF vs HF-Kt; "f"—HF vs HF-Kt

by food-restriction ($P \leq .05$), indicated by the symbol "#" (Figure 2A-E.). This feeding to food-restricted induction of lipid oxidation was blunted in HF livers. However, carbohydrate restriction and supplementation of BCAAs resulted in a fed to food-restricted induction of hepatic lipid oxidation ("#"; $P \leq .05$; Figure 2A-E.). This trend is also demonstrated by the higher Fed to Food-restricted fold change in expression of all the lipid oxidation genes in the HF-Kt mice livers compared to their HF counterparts ("c"; $P \leq .05$; Figure 2A-E.). We also determined the levels of hepatic acyl-carnitines (Figure 2F.), which are known to be elevated in mice with NAFLD, indicating inefficient lipid oxidation.[8] Elevated

levels of acyl-carnitines were evident in the HF mice livers compared to their LF counterparts, though only statistically significant for the C6 acylcarnitine. The ketogenic diet (HF-Kt) lowered hepatic acyl-carnitine levels relative to their HF counterparts, consistent with the idea that higher rates of lipid oxidation can relieve the accumulation of longer chain acylcarnitines in the liver. While this decrease was consistent across all the acyl-carnitines between HF and HF-Kt group, it was statistically significant only for C14 (Figure 2.F.). Taken together, these results indicate the ketogenic dietary environment helped sustain higher rates of free fatty acid oxidation in the liver, and in turn higher rates of ketogenesis.

3.4 | The ketogenic environment selectively altered reactions of the hepatic TCA cycle

Basal oxygen consumption rates for the mitochondria from HF-Kt livers were not significantly different from their LF or HF counterparts. However, ADP stimulated respiration rates were higher in the HF-Kt liver mitochondria compared to their LF ($P \leq .05$) and HF ($P \leq .1$) counterparts (Figure 3B.). We then determined whether higher rates of O_2 consumption by the HF-Kt liver mitochondria translated into higher rates of TCA cycle activity. Rates of biochemical reactions in the TCA cycle (Figure 3A.) were determined from the metabolite pool sizes (Supporting Table S3) and the mass isotopomer distribution arising from [$^{13}C_3$]pyruvate (Supporting Figure S1), using Isotopomer Network Compartmental Analysis (INCA).[26] The rate of entry of pyruvate into the mitochondrial matrix (*v1*) remained similar between mitochondria from all the three groups (Figure 3C.). However, the formation of oxaloacetate from pyruvate, an index of pyruvate carboxylase activity (*v2*) trended to be higher ($P \leq .1$) in HF-Kt liver mitochondria, compared to LF liver mitochondria (Figure 3C.). Conversion of pyruvate to acetyl-CoA, a reflection of pyruvate dehydrogenase activity (*v3*), remained similar between all the three groups (Figure 3C.). Estimates of ketogenesis (*v4*) derived through INCA demonstrated higher flux in mitochondrial derived from HF-Kt mice (Figure 3D.). Modeling of citrate synthase flux (*v5*) revealed an interesting trend in that HF-Kt diets downregulated *v5,* relative to their HF counterparts. Consistent with previous studies,[1,2,8] mitochondria derived from HF mice had significantly higher *v5* relative to their LF counterparts (Figure 3E.). In spite of the lower flux through citrate synthase in HF-Kt mice, formation of α-ketoglutarate from citrate (*v6;* aconitase + isocitrate dehydrogenase flux), formation of succinate from α-ketoglutarate (*v7*; α-ketoglutarate dehydrogenase flux), reversible conversion of succinate to fumarate (*v8*; succinate dehydrogenase flux) and the reversible conversion of fumarate to malate (*v9*; fumarase flux) were all significantly higher ($P \leq .05$) in the HF-Kt liver mitochondria compared to both LF and HF groups (Figure 3E.). Conversion of malate to oxaloacetate (*v10*; malate dehydrogenase flux) was higher in HF mice relative to their LF counterparts, but HF-Kt diet downregulated this flux, compared to the HF group (Figure 3E.). Higher fold changes in concentrations of hepatic mitochondrial TCA cycle intermediates from "Fed" to "Food-restricted" in the HF-Kt group lends support to the idea that the ketogenic environment could be selectively upregulating flux through the TCA cycle (Supporting Figure S2A-E). In summary, the ketogenic diet predisposes the mitochondria to elevated flux through the redox dependent reactions at isocitrate dehydrogenase, α-ketoglutarate dehydrogenase and succinate dehydrogenase, while flux through citrate synthase and malate dehydrogenase reactions seem to be downregulated.

Mitochondrial electron micrographs suggest that the overall induction of the oxidative machinery in the HF-Kt mice could be modulated by changes in mitochondrial morphology and number. The electron micrographs illustrate more rounded mitochondria in the HF hepatocytes compared to more elongated mitochondria in the LF and HF-Kt livers (Supporting Figure S3A). Furthermore, there is a trend ($P \leq .1$) toward higher number of mitochondria in the HF-Kt hepatocytes (Supporting Figure S3B), while the total mitochondrial surface area remained the same (Supporting Figure S3C).

3.5 | Ketogenic diet suppressed de novo lipogenesis in the liver

Deuterium incorporation into newly synthesized lipids in the liver was determined utilizing ^{2}H NMR (Figure 4A.). As expected, deuterium enrichments in the methyl peaks of the lipids (Figure 4B.) and the calculated rates of de novo lipogenesis (Figure 4C.) were significantly lower ($P \leq .05$) in the HF group compared to their LF counterparts. More interestingly, deuterium enrichments in the methyl peaks of the lipids (Figure 4B.) and the calculated rates of de novo lipogenesis (Figure 4C.) were significantly lower in the HF-Kt group ($P \leq .05$) compared to their HF and LF counterparts. A similar trend was evident with lipogenic gene expression in the liver (Figure 4D.), even though statistically significant decrease ($P \leq .05$) was achieved between HF and HF-Kt groups only for *Scd1* expression.

3.6 | Ketogenic diet-associated metabolic remodeling did not improve tissue specific insulin resistance

To determine whether the above detailed metabolic responses resulted in improvements in tissue specific indices of insulin resistance, we conducted a hyperinsulinemic

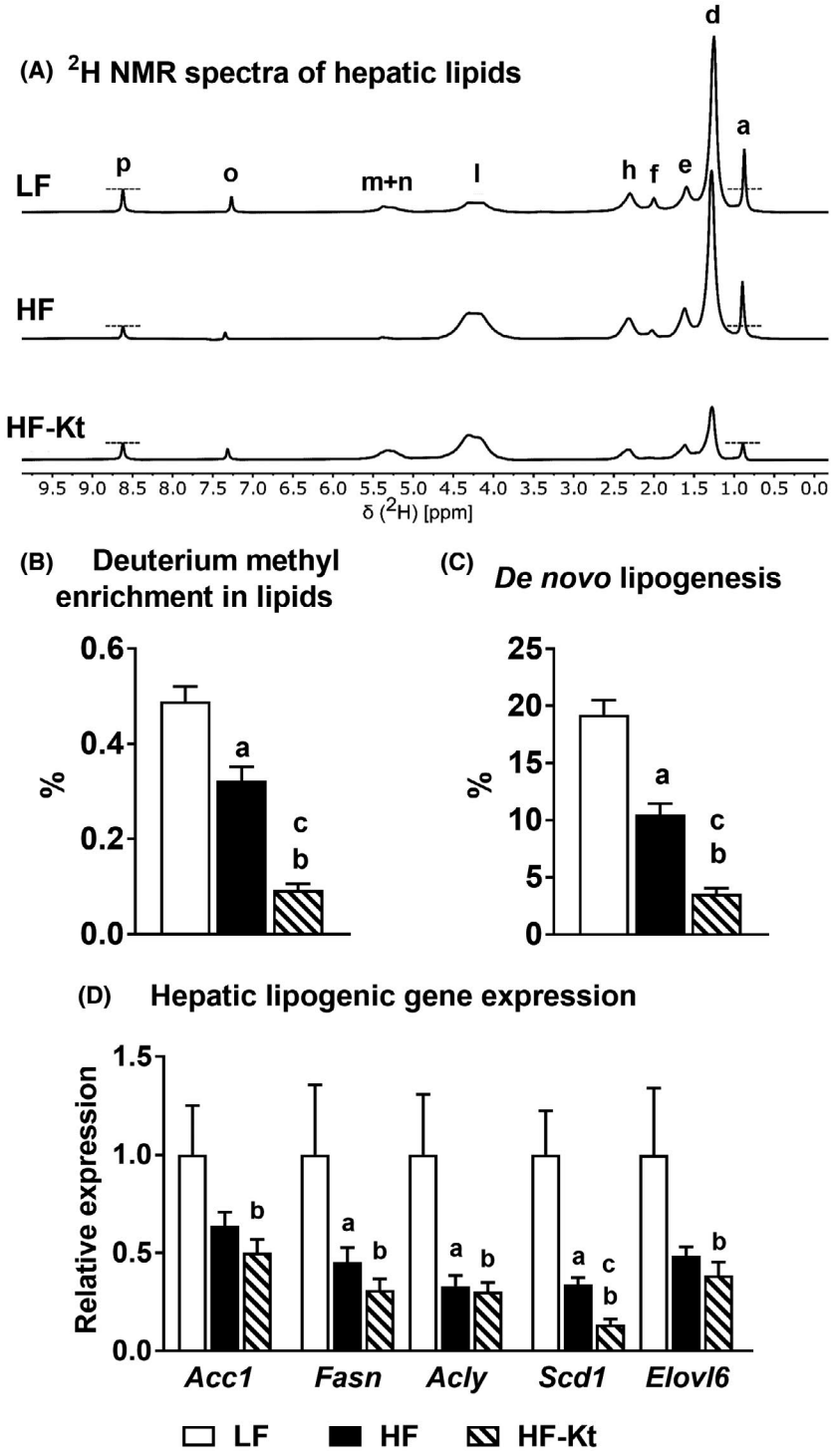

FIGURE 4 The ketogenic dietary environment suppressed hepatic de novo lipogenesis. A, Representative ^{2}H NMR spectra of the Folch extracted lipids from the liver of LF, HF and HF-Kt mice. Assignments of marked peaks on the spectrum are as follows: (a) ω-3 methyl, (d) aliphatic chain, (e) α3 aliphatic, (f) monounsaturated allylic (h) All α2 aliphatic (l) sn-1, sn-3 of esterified glycerol, (m) sn-2 of esterified glycerol, (n) olefinic (o) chloroform and (p) pyrazine standard. Dotted lines on pyrazine (p) and methyl (a) peaks are showing the level of deuterium enrichment on the terminal methyl position in each of the sample, which ultimately gives the qualitative information of the de novo lipogenesis. B, Measured enrichment of deuterium in the methyl peaks of lipids, (C) Hepatic de novo lipogenesis and (D) Lipogenic gene expression in the liver. Results (n = 5-6/group) were considered significant at $P \leq .05$ following pairwise mean comparisons which are represented by the following alphabets. "a"—LF vs HF; "b"—LF vs HF-Kt; "c"—HF vs HF-Kt

euglycemic clamp. The endogenous glucose production (EGP) under both food-restricted and insulin stimulated states remained similar between HF and HF-Kt groups, but were significantly higher ($P \leq .05$) compared to their LF counterparts (Figure 5A.). The percent suppression of EGP (Figure 5B.) and serum FFAs (Figure 5C.) by insulin were significantly blunted ($P \leq .05$) in both the HF and HF-Kt groups. Furthermore, hepatic insulin resistance index (Figure 5D.), glucose disposal rate which is a reflection of muscle insulin resistance (Figure 5E.) and adipose tissue insulin resistance index (Figure 5F.), all demonstrated a significantly higher degree of insulin resistance ($P \leq .05$) in both HF and HF-Kt groups, with not change between HF and HF-Kt groups. Insulin stimulation induced significant phosphorylation of AKT in the livers from the LF group (Figure 5G.). However, the phosphorylation rates of AKT in response to insulin were blunted in both the HF and HF-Kt groups (Figure 5G.). Over all, these results suggest that the ketogenic environment did not alleviate insulin resistance during NAFLD.

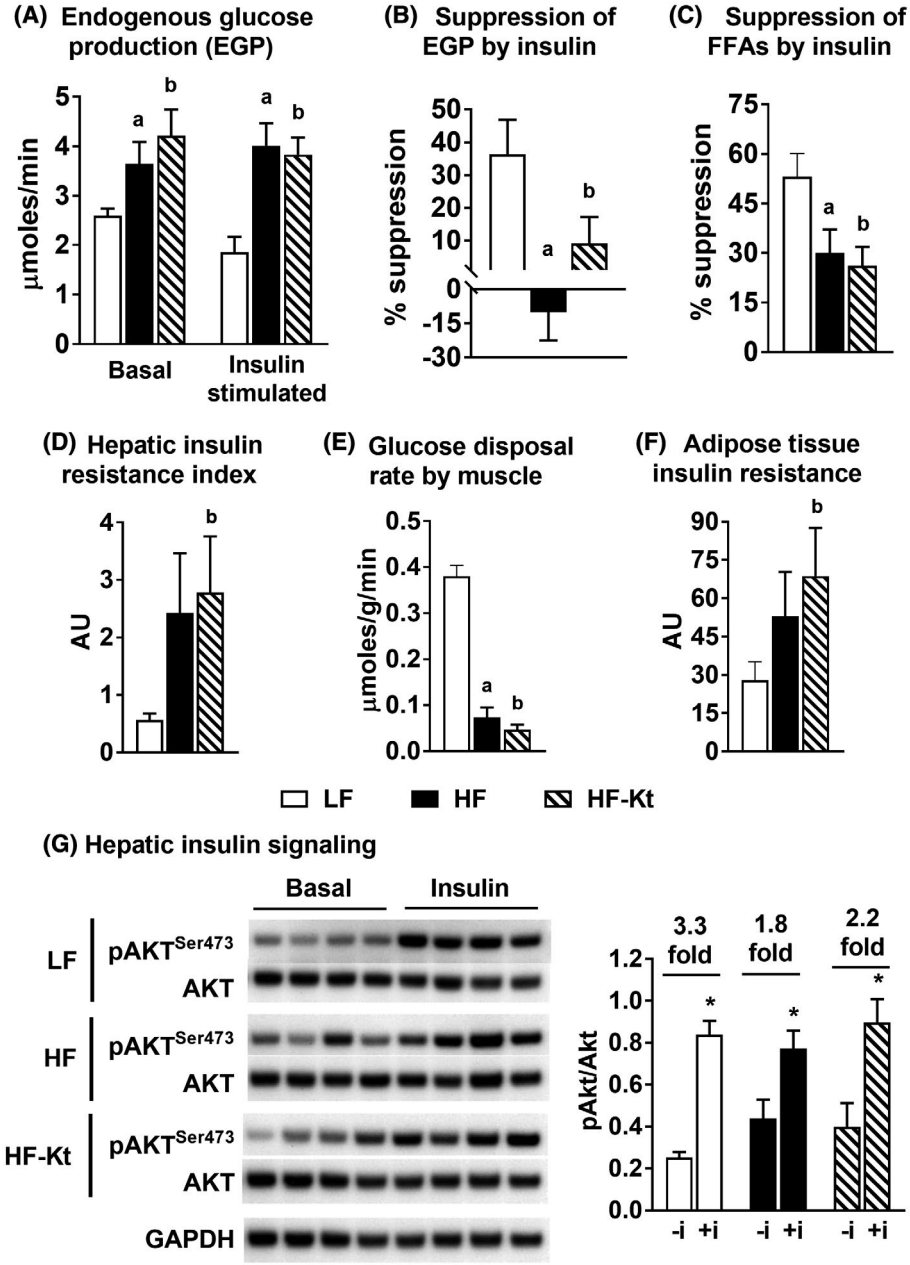

FIGURE 5 The metabolic remodeling mediated by the ketogenic environment did not translate to improvements in insulin sensitivity. A, Endogenous glucose production (EGP) during food-restricted (basal) and insulin stimulated states. B, Suppression of EGP by insulin. C, Suppression of plasma FFAs by insulin. D, Hepatic insulin sensitivity index, calculated as the product of fasting EGP and fasting serum insulin. E, Glucose disposal rate, which is a reflection of muscle insulin sensitivity (F). Adipose insulin sensitivity index, calculated as the product of fasting FFAs and fasting serum insulin. G, Phosphorylation rates of AKT in the liver, and their fold increase following insulin stimulation. Results (n = 5-8/group) were considered significant at $P \leq .05$ following pairwise mean comparisons which are represented by the following alphabets. "a"—LF vs HF; "b"—LF vs HF-Kt; "c"—HF vs HF-Kt. "*"—indicates statistical significance at $P \leq .05$ using a Student's t test between means of basal and insulin stimulated groups

3.7 | The ketogenic environment aggravated metabolic dysfunction during NAFLD

"Food-restricted" liver histology (Figure 6A.) and liver triglyceride measurements (Table 1) reveal that lipid accumulation is significantly higher in the HF-Kt group compared to mice reared on a HF diet. This was further confirmed by an independent pathologist with the lipid accumulation in the liver of the food-restricted HF animals significantly lower than their HF-Kt counterparts (Steatosis score of 1.3 for HF vs 3 for HF-Kt, on a scale of 0-4; 0 being normal and 4 being severe). Serum ALT levels following food-restriction tended to be higher in the HF-Kt mice compared to their HF counterparts (Figure 6B). Furthermore, fibrogenic gene expression

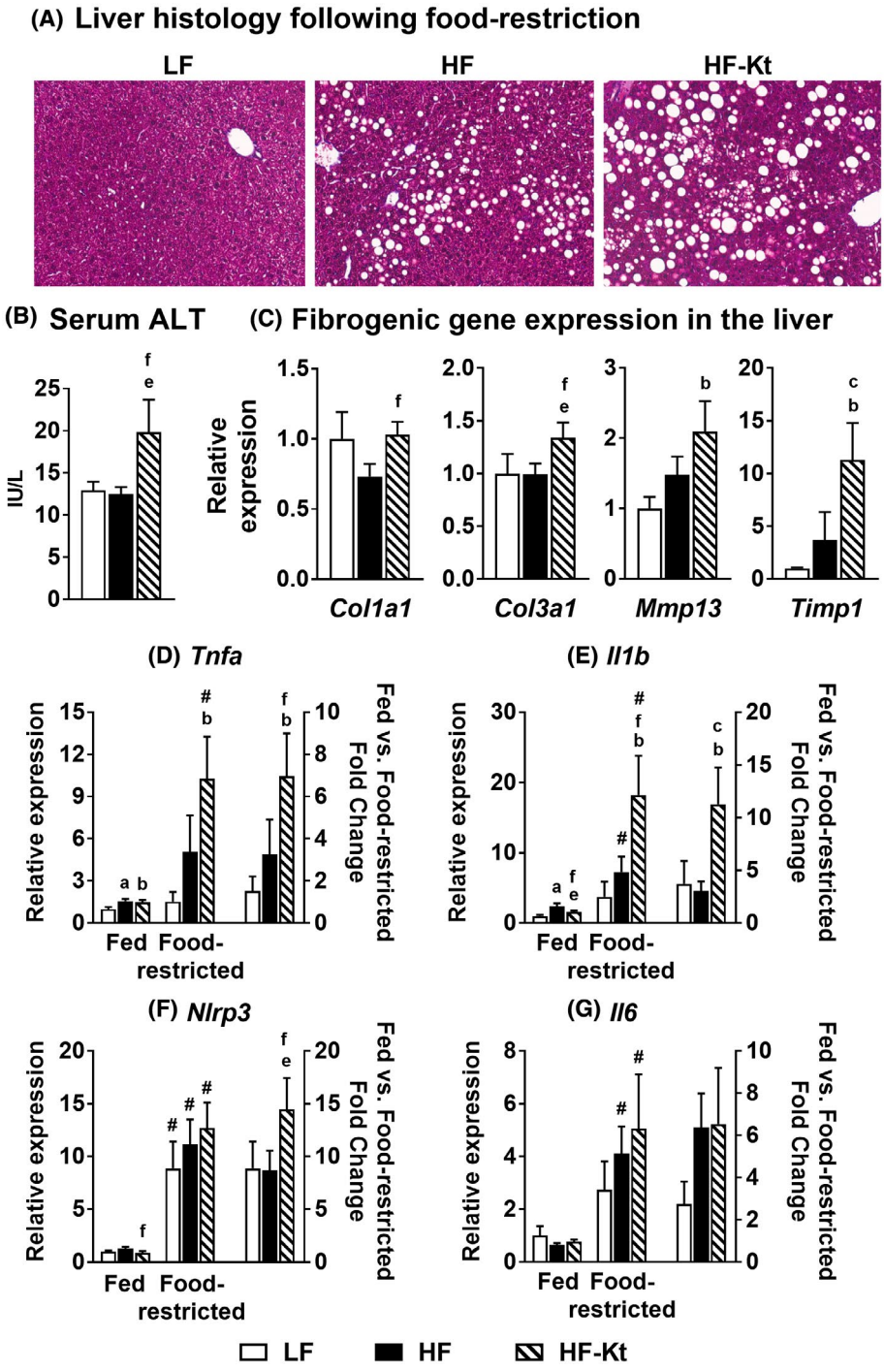

FIGURE 6 Chronic exposure to the ketogenic environment accelerates liver injury during NAFLD. A, Masson's Trichrome staining of liver tissue following food-restriction. B, Fasting serum Alanine Aminotransferase (ALT) levels. C, Hepatic fibrogenic gene expression profiles after food-restriction. Fed and food-restricted expression profiles of genes involved in the inflammatory on set in the liver. D, *Tnfa*, Tumor necrosis factor alpha (E) *Il1b*, Interleukin 1 beta (F) *Nlrp3,* NLR family, pyrin domain containing 3 and (G) *Il6*. Interleukin 6. Results (n = 5-8/group) were considered significant at $P \leq .05$ following pairwise mean comparisons which are represented by the following alphabets. "a"—LF vs HF; "b"—LF vs HF-Kt; "c"—HF vs HF-Kt. Results which are significant at $P \leq .1$ following pairwise mean comparisons are represented by the following alphabets. "d"—LF vs HF; "e"—LF vs HF-Kt; "f"—HF vs HF-Kt. "#"—indicates statistical significance at $P \leq .05$ using a Student's t test between means of the fed and food-restricted groups

measured in livers collected from food-restricted mice, an index of progressive severity of NAFLD, tended to be higher in the HF-Kt group (Figure 6C.). However, evaluation of liver histology based on Masson's Trichrome staining (Figure 6A.) by an independent pathologist did not show any evidence of fibrosis in any of the three groups. Expression profiles of

canonical genes involved in inflammatory networks (*Tnfa*, *Il1b*, *Nlrp3,* and *Il6*) when profiled under "Fed" and "Food-restricted" conditions demonstrate a higher fold "Fed" to "Food-restricted" induction with the chronic ketogenic environment (Figure 6D-G.). Furthermore, mitochondrial ROS generation was higher in the "Fed" HF-Kt group (Supporting Figure S4A), even though ROS generation rates remained similar between groups under "Food-restricted" conditions (Supporting Figure S4B). Altogether, these results coupled with severe insulin resistance evident in the HF-Kt mice, points to the progressive severity of NAFLD.

4 | DISCUSSION

The biochemical coupling of mitochondrial oxidative networks (β-oxidation, ketogenesis and TCA cycle flux) with OXPHOS and ATP synthesis generates ROS as a normal metabolic byproduct.[9,33] However, in the setting of hepatic insulin resistance and NAFLD, mitochondrial oxidative fluxes undergoes dynamic remodeling, altering the normal redox balance. During initial stages of NAFLD, several oxidative fluxes undergoes a compensatory induction, while during later stages and with progressive severity of NAFLD, certain oxidative fluxes become dysfunctional and impaired.[2,3,34] This occur concurrently with sustained ROS production, oxidative stress and inflammatory onset.[4,5,9] We and others have shown previously that ketogenesis is one of the major pathways which undergoes an initial compensatory induction followed by a later impairment during progression of NAFLD.[2,7,35] We hypothesized that (a) 16-wks of HF diet feeding and the progressive severity of hepatic insulin resistance will blunt ketogenic flux and (b) supplementation of BCAAs by replacing carbohydrate calories (HF-Kt) on a HF diet background, will revive ketogenic flux. In fact, our results illustrate that 16-wks of HF feeding blunted ketogenic flux, which was revived by the chronic ketogenic environment generated by the HF-Kt diet (Figure 1). This allowed us to investigate the impact of chronic ketogenic environment on hepatic mitochondrial oxidative function, insulin sensitivity and cellular stress, under the setting of NAFLD. The evaluation of ketogenic flux was conducted based on the turnover rates of β-hydroxybutyrate. Here it is pertinent to mention that the flux of acetoacetate, the other major ketone was not measured in this study under the expectation that the changes in the flux of acetoacetate will parallel that of β-hydroxybutyrate. However, the measurement of acetoacetate could have yielded valuable insights into the NADH and NAD+ ratios and the energy status of the cell, as the interconversion of acetoacetate and β-hydroxybutyrate occurs through reduction-oxidation reactions using NADH and NAD+.[36,37]

The ketogenic environment generated by the HF-Kt dietary regimen in this study was in fact fueled by the induction of lipid oxidation as illustrated by the "Fed" to "Food-restricted" fold changes in the associated genes (Figure 2). Ketogenic macronutrient milieu which "burns fat" through lipid oxidation is extensively used as a strategy for preventing excess lipid accumulation during obesity and NAFLD.[12,38] While several benefits of ketogenic diets have been documented in humans and mice models with NAFLD, there is ambiguity about these diets long-term impacts on hepato-cellular function.[11,17,19-21,39] Biochemically, ketogenesis is the reflection of surplus acetyl-CoA from FFA oxidation, getting diverted away from complete oxidation through the TCA cycle, toward the synthesis of ketones. In other words, the ketogenic environment upregulates components of mitochondrial oxidative machinery in the liver (eg, β-oxidation, ketone synthesis). We show here that this rather simple appreciation of the ketogenic diet lacks the detail necessary to explain all the phenomena observed here. This aspect is particularly significant considering the wide variety of macronutrient compositions which could be ketogenic. In this study, we hypothesized that the BCAAs together with restricted availability of carbohydrates will create a unique ketogenic environment which will exacerbate mitochondrial oxidative dysfunction in the liver. Considering the already evident dysfunctional redox balance in the liver during NAFLD, it is unclear whether chronic upregulation of components of mitochondrial oxidative machinery is a beneficial strategy to avoid progressive lipid accumulation and alleviate cellular stress during NAFLD.

A major component of mitochondrial oxidative function is the TCA cycle, which is not only responsible for the complete oxidation of acetyl-CoA to CO_2, but it also supports anaplerotic and cataplerotic reactions required for biosynthetic reactions (eg, gluconeogenesis, lipogenesis etc). Sustained hepatic TCA cycle activity has been documented in humans and rodent models with NAFLD,[1,2] and further more have been linked to inflammatory onset and oxidative stress.[9] To evaluate the impact of the ketogenic environment on TCA cycle activity, we incubated isolated hepatic mitochondria with [$^{13}C_3$]pyruvate. Isotopomer Network Compartmental Analysis (INCA) revealed a lower rate of citrate synthase flux under the ketogenic environment (*v5*; Figure 3E). Interestingly, INCA also revealed that the fluxes through the redox dependent reactions at isocitrate dehydrogenase, α-ketoglutarate dehydrogenase and succinate dehydrogenase were elevated, despite lower citrate synthase flux in HF-Kt mice. Essential points to keep in mind are that we are not at metabolic or isotopic steady state. The INCA simulations that produce the fluxes are kinetic in nature, and make no steady state assumptions. This approach demands inclusion of the finite pool sizes. In addition, the presence of malate in the media can foster

exchange through the malate citrate carrier, and also can serve as a pool which dilutes the ^{13}C labeling in the mitochondria. Hence, malate enrichment is lower than both fumarate and aspartate (Supporting Figure S1). In this condition, it is not expected that flux through citrate synthase should be equal to flux throughout other steps of the TCA cycle, as the span of the TCA cycle from malate to citrate is essentially isolated from the rest of the cycle by the experimental conditions. It is possible that if cataplerotic and anaplerotic reactions are connected via subsequent TCA cycle intermediates, then flux through individual steps of the cycle can exceed flux through other reactions.[40] The addition of exogenous malate appears to exert control over the malate-citrate carrier, as flux through malate dehydrogenase and citrate synthase is equivalent. For every malate imported, a citrate is exported, and flux through the intervening enzymatic reactions must be conserved. However, without the fully operational malate-aspartate shuttle, glutamate and aspartate pool sizes drop precipitously on addition of malate (Supporting Table S3). These changes in pool size enable the observed differences in flux observed throughout the TCA cycle (Figure 3.). HF-Kt feeding resulted in hepatic mitochondria upregulating lipid oxidation and ketone production (Figures 1, 2 and 3D.). Acetyl-CoA mass balance was conserved, as downregulation of citrate synthase flux compensated for changes in lipid oxidation and ketone production. Upregulation of NADH producing steps of the TCA cycle (*v6-v8*, Figure 3.) were driven by the O_2 consumption, used as a parameter within the INCA simulation, as well as by the observed fractional enrichments (Supporting Figure S1). This hyper-activated oxidative flux has been correlated with inflammation in previous studies.[2,8,9] A better summary of the ketogenic diet is that it provides a surplus of non-carbohydrate sources of acetyl-CoA production, which ultimately is correlated with increased NADH production from the lower span of the TCA cycle (Figure 3.). It remains unclear if the experimental preparation using isolated mitochondria enforces changes in citrate synthase flux that would not hold in the in vivo liver. From a whole body perspective, de novo lipogenesis in the liver was significantly lower in the mice reared on the ketogenic diet. In fact various metabolic milieu which promotes ketogenesis have been shown to down regulate de novo lipogenesis in the liver.[21,41,42] Taken together, these results suggest that the ketogenic environment is primed to shunt the majority of the acetyl-CoA into ketogenesis and away from both citrate synthase flux and export into the cytoplasm for serving as a substrate for de novo lipogenesis.

It is clear from the above discussion that chronic ketogenic environment under a NAFLD setting, resulted in an overall induction of mitochondrial oxidative function in mouse liver. Under "Fed" conditions, the HF-Kt mice had lower liver weights, decreased liver triglycerides and lower levels of serum insulin (Table 1) suggesting that the ketogenic milieu was blunting the progression of NAFLD. However, food-restricted mice on HF-Kt diet, had a higher degree of lipid accumulation in the liver (Table 1; Figure 6), higher liver weights and similar insulin levels, compared to their HF diet counterparts (Table 1). These results demonstrated a greater degree of "inflexibility" for the mice on the HF-Kt diets to switch from a "Fed" to "Food-restricted" metabolic phenotype. Furthermore, the mice on the HF diet were severely insulin resistant and the ketogenic environment did not result in any improvements in liver, muscle or adipose insulin resistance (Figure 5). Inflammatory and fibrogenic gene expression in the liver also trended to be higher with the chronic ketogenic environment (Figure 6). Consistent with our findings, prolonged exposure of ketogenic environment have been shown to induce hepatic steatosis, inflammation, endoplasmic reticulum stress, elevated liver enzymes, and higher cholesterol.[19,38,43,44] Multiple mechanisms could be at play in promoting this pro-inflammatory metabolic phenotype during food-restriction. First, under the presumption that oxidative activity will be higher during food-restriction, the interaction between the sustained mitochondrial oxidative flux, chronic ROS production and inflammation can contribute to the progressive severity of NAFLD.[2,8,9] Of particular interest is the succinate dehydrogenase reaction (*v8*; Figure 3E) which occurs within Complex II of the respiratory complex. Whether oxidative damage within Complex II[45,46] is the mechanism underlying this metabolic dysfunction is to be determined. Second, prolonged exposure to the ketone bodies could elicit pro-inflammatory signaling cascades.[47-49] Third, the role of BCAAs needs to be further investigated, as recent literature highlights the close interaction between BCAAs, lipid metabolism, and insulin resistance[13,14,16] and furthermore their potential to elicit oxidative stress and accelerate liver injury.[50-52] Here it is also relevant to note that the HF-Kt mice had a higher degree of adiposity, contrary to our expectations, as a ketogenic environment could reliably be expected to reduce body weight. However, with the emerging literature illustrating close interactions between BCAAs and pathways of lipid metabolism including lipogenesis, lipolysis[51,53]; a significant role of BCAAs in the manifestation of the metabolic phenotype exhibited by the HF-Kt animals, cannot be ruled out.

In summary, our results suggest that chronic ketogenic environment under a setting of NAFLD helps to sustain higher rates of mitochondrial oxidative metabolism in the liver through β-oxidation, ketogenesis and discrete biochemical reactions in the TCA cycle (Figure 7). The ketogenic metabolic milieu shunts 2-carbon units of acetyl-coA predominantly toward ketone synthesis, and away from de novo lipogenesis and citrate synthase reaction in the liver. While

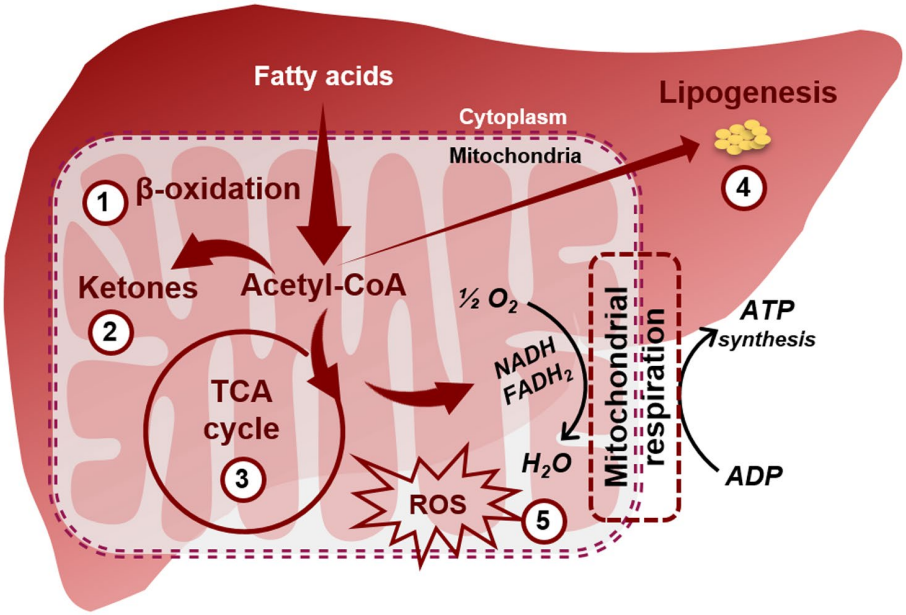

FIGURE 7 Impact of chronic ketogenic environment on mitochondrial metabolism, lipogenesis, and oxidative stress during NAFLD. A ketogenic environment mediates sustained rates of oxidation of free fatty acids in the liver (1) generating 2-carbon units of acetyl-coA, which are shunted toward ketone synthesis (2) with selective upregulation of biochemical reactions in the TCA cycle (3). This chronic metabolic adaptation by the mitochondrial oxidative machinery occurs simultaneously with the downregulation of acetyl-CoA flux to de novo lipogenesis (4). The sustained induction of mitochondrial oxidative metabolism in the liver provides a favorable environment for the sustained generation of ROS (5) fueling higher rates of inflammation, in turn aggravating hepatic injury during NAFLD

lower rates of lipogenesis could be conceived as an overall beneficial phenotype, under conditions of high oxidative flux in the liver, it could increase the susceptibility of the hepatocyte to oxidative damage. Thus, chronic exposure to a ketogenic milieu seem to provide a favorable environment for continuous, subclinical generation of ROS, higher rates of inflammation and persistent hepatic insulin resistance. In conclusion, continuous exposure to a ketogenic environment and the resultant sustained induction of the oxidative machinery could present a significant risk toward aggravating liver injury during NAFLD.

ACKNOWLEDGMENTS

We are grateful to Tim Maugel at the Laboratory for Biological Ultrastructure, University of Maryland, College Park, MD for the transmission electron microscopy of liver mitochondria. We are grateful to Timothy J. Garrett and Joy G. Cagmat at the Southeast Center for Integrated Metabolomics at University of Florida, Gainesville for the LC-MS/MS analysis of acylcarnitines. The work was supported by National Institutes of Health (NIH) grant RO1-DK-112865 (to NES). A portion of this work was performed at the National High Magnetic Field Laboratory, supported by the National Science Foundation Cooperative Agreement number DMR-1644779, & the State of Florida. MM acknowledges support from NIH P41-122698, 5U2CDK119889, and NIH R01-105346.

CONFLICT OF INTEREST

The authors declare no conflicts of interest.

AUTHOR CONTRIBUTIONS

N.E. Sunny conceived and designed the study; N.E. Sunny, M.S. Muyyarikkandy, M. Maguire, R. Mahar, C. Surugihalli, C. Zhang, N. Kattapuram and V. Muralidaran performed the experiments; N.E. Sunny, M.E. Merritt, C.E. Mathews, M.S. Muyyarikkandy, M. McLeod, M. Maguire, R. Mahar and K. Vavilikolanu analyzed the data; N.E. Sunny, M.E. Merritt, M.S. Muyyarikkandy, M. McLeod and R. Mahar wrote the manuscript; N.E. Sunny, M.E. Merritt and C.E. Mathews acquired funding.

REFERENCES

1. Sunny NE, Parks EJ, Browning JD, Burgess SC. Excessive hepatic mitochondrial TCA cycle and gluconeogenesis in humans with nonalcoholic fatty liver disease. *Cell Metab*. 2011;14:804-810.
2. Satapati S, Sunny NE, Kucejova B, et al. Elevated TCA cycle function in the pathology of diet-induced hepatic insulin resistance and fatty liver. *J Lipid Res*. 2012;53:1080-1092.
3. Koliaki C, Szendroedi J, Kaul K, et al. Adaptation of hepatic mitochondrial function in humans with non-alcoholic fatty liver is lost in steatohepatitis. *Cell Metab*. 2015;21:739-746.
4. Begriche K, Massart J, Robin MA, Bonnet F, Fromenty B. Mitochondrial adaptations and dysfunctions in nonalcoholic fatty liver disease. *Hepatology*. 2013;58:1497-1507.

5. Boland ML, Oldham S, Boland BB, et al. Nonalcoholic steatohepatitis severity is defined by a failure in compensatory antioxidant capacity in the setting of mitochondrial dysfunction. *World J Gastroenterol*. 2018;24:1748-1765.
6. Sunny NE, Bril F, Cusi K. Mitochondrial adaptation in nonalcoholic fatty liver disease: novel mechanisms and treatment strategies. *Trends Endocrinol Metab*. 2017;28:250-260.
7. Sunny NE, Satapati S, Fu X, et al. Progressive adaptation of hepatic ketogenesis in mice fed a high-fat diet. *Am J Physiol Endocrinol Metab*. 2010;298:E1226-E1235.
8. Patterson RE, Kalavalapalli S, Williams CM, et al. Lipotoxicity in steatohepatitis occurs despite an increase in tricarboxylic acid cycle activity. *Am J Physiol Endocrinol Metab*. 2016;310:E484-E494.
9. Satapati S, Kucejova B, Duarte JA, et al. Mitochondrial metabolism mediates oxidative stress and inflammation in fatty liver. *J Clin Investig*. 2016;126:1605.
10. Abbasi J. Interest in the ketogenic diet grows for weight loss and type 2 diabetes. *JAMA*. 2018;319:215-217.
11. Trimboli P, Castellana M, Bellido D, Casanueva FF. Confusion in the nomenclature of ketogenic diets blurs evidence. *Rev Endocr Metab Disord*. 2020;21:1-3.
12. Caprio M, Infante M, Moriconi E, et al. Very-low-calorie ketogenic diet (VLCKD) in the management of metabolic diseases: systematic review and consensus statement from the Italian Society of Endocrinology (SIE). *J Endocrinol Invest*. 2019;42:1365-1386.
13. Kujala UM, Peltonen M, Laine MK, et al. Branched-chain amino acid levels are related with surrogates of disturbed lipid metabolism among older men. *Front Med*. 2016;3:57.
14. Lerin C, Goldfine AB, Boes T, et al. Defects in muscle branched-chain amino acid oxidation contribute to impaired lipid metabolism. *Mol Metab*. 2016;5:926-936.
15. Li T, Zhang Z, Kolwicz SC Jr, et al. Defective branched-chain amino acid catabolism disrupts glucose metabolism and sensitizes the heart to ischemia-reperfusion injury. *Cell Metab*. 2017;25:374-385.
16. Sunny NE, Kalavalapalli S, Bril F, et al. Cross-talk between branched-chain amino acids and hepatic mitochondria is compromised in nonalcoholic fatty liver disease. *Am J Physiol Endocrinol Metab*. 2015;309:E311-E319.
17. Belopolsky Y, Khan MQ, Sonnenberg A, Davidson DJ, Fimmel CJ. Ketogenic, hypocaloric diet improves nonalcoholic steatohepatitis. *J Transl Int Med*. 2020;8:26-31.
18. Cotter DG, Ercal B, Huang X, et al. Ketogenesis prevents diet-induced fatty liver injury and hyperglycemia. *J Clin Invest*. 2014;124:5175-5190.
19. Garbow JR, Doherty JM, Schugar RC, et al. Hepatic steatosis, inflammation, and ER stress in mice maintained long term on a very low-carbohydrate ketogenic diet. *Am J Physiol Gastrointest Liver Physiol*. 2011;300:G956-G967.
20. Joshi S, Ostfeld RJ, McMacken M. The ketogenic diet for obesity and diabetes-enthusiasm outpaces evidence. *JAMA Intern Med*. 2019;179:1163.
21. Luukkonen PK, Dufour S, Lyu K, et al. Effect of a ketogenic diet on hepatic steatosis and hepatic mitochondrial metabolism in nonalcoholic fatty liver disease. *Proc Natl Acad Sci U S A*. 2020;117:7347-7354.
22. Rosenbaum M, Hall KD, Guo J, et al. Glucose and lipid homeostasis and inflammation in humans following an isocaloric ketogenic diet. *Obesity (Silver Spring)*. 2019;27:971-981.
23. Musso G, Gambino R, Cassader M, Pagano G. Meta-analysis: natural history of non-alcoholic fatty liver disease (NAFLD) and diagnostic accuracy of non-invasive tests for liver disease severity. *Ann Med*. 2011;43:617-649.
24. Rinella ME. Nonalcoholic fatty liver disease: a systematic review. *JAMA*. 2015;313:2263-2273.
25. Sunny NE, Bequette BJ. Glycerol is a major substrate for glucose, glycogen, and nonessential amino acid synthesis in late-term chicken embryos1,2,3. *J Anim Sci*. 2011;89:3945-3953.
26. Young JD. INCA: a computational platform for isotopically non-stationary metabolic flux analysis. *Bioinformatics*. 2014;30:1333-1335.
27. Fernandez CA, Des Rosiers C, Previs SF, David F, Brunengraber H. Correction of 13C mass isotopomer distributions for natural stable isotope abundance. *J Mass Spectrom*. 1996;31:255-262.
28. Delgado TC, Pinheiro D, Caldeira M, et al. Sources of hepatic triglyceride accumulation during high-fat feeding in the healthy rat. *NMR Biomed*. 2009;22:310-317.
29. Duarte JA, Carvalho F, Pearson M, et al. A high-fat diet suppresses de novo lipogenesis and desaturation but not elongation and triglyceride synthesis in mice. *J Lipid Res*. 2014;55:2541-2553.
30. Young JD, Walther JL, Antoniewicz MR, Yoo H, Stephanopoulos G. An elementary metabolite unit (EMU) based method of isotopically nonstationary flux analysis. *Biotechnol Bioeng*. 2008;99:686-699.
31. Antoniewicz MR, Kelleher JK, Stephanopoulos G. Determination of confidence intervals of metabolic fluxes estimated from stable isotope measurements. *Metab Eng*. 2006;8:324-337.
32. Crown SB, Long CP, Antoniewicz MR. Integrated 13C-metabolic flux analysis of 14 parallel labeling experiments in *Escherichia coli*. *Metab Eng*. 2015;28:151-158.
33. Forrester SJ, Kikuchi DS, Hernandes MS, Xu Q, Griendling KK. Reactive oxygen species in metabolic and inflammatory signaling. *Circ Res*. 2018;122:877-902.
34. Schmid AI, Szendroedi J, Chmelik M, Krssak M, Moser E, Roden M. Liver ATP synthesis is lower and relates to insulin sensitivity in patients with type 2 diabetes. *Diabetes Care*. 2011;34:448-453.
35. Fletcher JA, Deja S, Satapati S, Fu X, Burgess SC, Browning JD. Impaired ketogenesis and increased acetyl-CoA oxidation promote hyperglycemia in human fatty liver. *JCI Insight*. 2019;5:e127737.
36. Xin L, Ipek O, Beaumont M, et al. Nutritional ketosis increases NAD(+)/NADH ratio in healthy human brain: an in vivo study by (31)P-MRS. *Front Nutr*. 2018;5:62.
37. Puchalska P, Crawford PA. Multi-dimensional roles of ketone bodies in fuel metabolism, signaling, and therapeutics. *Cell Metab*. 2017;25:262-284.
38. Schugar RC, Crawford PA. Low-carbohydrate ketogenic diets, glucose homeostasis, and nonalcoholic fatty liver disease. *Curr Opin Clin Nutr Metab Care*. 2012;15:374-380.
39. Moore MP, Cunningham RP, Kelty TJ, et al. Ketogenic diet in combination with voluntary exercise impacts markers of hepatic metabolism and oxidative stress in male and female Wistar rats. *Appl Physiol Nutr Metab*. 2020;45:35-44.
40. Ragavan M, Kirpich A, Fu X, Burgess SC, McIntyre LM, Merritt ME. A comprehensive analysis of myocardial substrate preference emphasizes the need for a synchronized fluxomic/

metabolomic research design. *Am J Physiol Heart Circ Physiol*. 2017;312:H1215-H1223.
41. Nishikata N, Shikata N, Kimura Y, Noguchi Y. Dietary lipid-dependent regulation of de novo lipogenesis and lipid partitioning by ketogenic essential amino acids in mice. *Nutr Diabetes*. 2011;1:e5.
42. Noguchi Y, Nishikata N, Shikata N, et al. Ketogenic essential amino acids modulate lipid synthetic pathways and prevent hepatic steatosis in mice. *PLoS One*. 2010;5:e12057.
43. Anekwe CV, Chandrasekaran P, Stanford FC. Ketogenic diet-induced elevated cholesterol, elevated liver enzymes and potential non-alcoholic fatty liver disease. *Cureus*. 2020;12:e6605.
44. Kosinski C, Jornayvaz FR. Effects of ketogenic diets on cardiovascular risk factors: evidence from animal and human studies. *Nutrients*. 2017;9:517.
45. Mills EL, Kelly B, Logan A, et al. Succinate dehydrogenase supports metabolic repurposing of mitochondria to drive inflammatory macrophages. *Cell*. 2016;167:457-470.e13.
46. Quinlan CL, Orr AL, Perevoshchikova IV, Treberg JR, Ackrell BA, Brand MD. Mitochondrial complex II can generate reactive oxygen species at high rates in both the forward and reverse reactions. *J Biol Chem*. 2012;287:27255-27264.
47. Kanikarla-Marie P, Jain SK. Hyperketonemia (acetoacetate) upregulates NADPH oxidase 4 and elevates oxidative stress, ICAM-1, and monocyte adhesivity in endothelial cells. *Cell Physiol Biochem*. 2015;35:364-373.
48. Jain SK, Kannan K, Lim G. Ketosis (acetoacetate) can generate oxygen radicals and cause increased lipid peroxidation and growth inhibition in human endothelial cells. *Free Radic Biol Med*. 1998;25:1083-1088.
49. Jain SK, Kannan K, Lim G, McVie R, Bocchini JA Jr. Hyperketonemia increases tumor necrosis factor-alpha secretion in cultured U937 monocytes and Type 1 diabetic patients and is apparently mediated by oxidative stress and cAMP deficiency. *Diabetes*. 2002;51:2287-2293.
50. Ericksen RE, Lim SL, McDonnell E, et al. Loss of BCAA catabolism during carcinogenesis enhances mTORC1 activity and promotes tumor development and progression. *Cell Metab*. 2019;29:1151-1165.e6.
51. Zhang F, Zhao S, Yan W, et al. Branched chain amino acids cause liver injury in obese/diabetic mice by promoting adipocyte lipolysis and inhibiting hepatic autophagy. *EBioMedicine*. 2016;13:157-167.
52. Zhenyukh O, Gonzalez-Amor M, Rodrigues-Diez RR, et al. Branched-chain amino acids promote endothelial dysfunction through increased reactive oxygen species generation and inflammation. *J Cell Mol Med*. 2018;22:4948-4962.
53. Green CR, Wallace M, Divakaruni AS, et al. Branched-chain amino acid catabolism fuels adipocyte differentiation and lipogenesis. *Nat Chem Biol*. 2016;12:15-21.

SUPPORTING INFORMATION

Additional Supporting Information may be found online in the Supporting Information section.

How to cite this article: Muyyarikkandy MS, McLeod M, Maguire M, et al. Branched chain amino acids and carbohydrate restriction exacerbate ketogenesis and hepatic mitochondrial oxidative dysfunction during NAFLD. *The FASEB Journal*. 2020;34:14832–14849. https://doi.org/10.1096/fj.202001495R